Cancer Detection Using a PET Tracer, ^{11}C-Glycylsarcosine, Targeted to H^+/Peptide Transporter

Keisuke Mitsuoka[1], Sosuke Miyoshi[2], Yukio Kato[1], Yoshihiro Murakami[2], Rie Utsumi[1], Yoshiyuki Kubo[1], Akihiro Noda[2], Yukio Nakamura[3], Shintaro Nishimura[2], and Akira Tsuji[1]

[1]Graduate School of Natural Science and Technology, Kanazawa University, Kakuma-machi, Kanazawa, Ishikawa, Japan; [2]The Medical and Pharmacological Research Center Foundation, Inoyama-chou, Hakui, Ishikawa, Japan; and [3]Cell Engineering Division, BioResource Center, RIKEN, Koyadai, Tsukuba, Ibaraki, Japan

H^+/peptide transporter, PEPT1, is functionally expressed in some human cancer cell lines and might be a candidate molecular target for detection of cancers in vivo using PET. The aim of the present study was to establish a novel tumor-imaging technology using a PET tracer targeted to H^+/peptide transporter(s). We also compared the tracer with ^{18}F-FDG, focusing on the specificity of their accumulation between tumor and inflammatory tissues. **Methods:** A dipeptide PET tracer, ^{11}C-glycylsarcosine (^{11}C-Gly-Sar), was injected intravenously into athymic mice transplanted with human pancreatic, prostate, and gastric cancer cells. The distribution patterns of ^{11}C-Gly-Sar and ^{18}F-FDG in the tumor-bearing mice, and in mice with inflammatory tissue, were assessed by imaging with a positron planar imaging system (PPIS). Tissue distributions of tracer radioactivity were also measured. The expression levels of PEPT1 and PEPT2 (PEPTs) proteins in tumor xenografts and inflammatory tissue were examined by immunohistochemical analysis. The messenger RNA expression levels of PEPTs in 58 available cancer cell lines were quantified by means of real-time polymerase chain reaction. **Results:** All 3 tumor xenografts were well visualized with the PPIS after injection of ^{11}C-Gly-Sar. Expression of PEPTs in those xenografts was confirmed by immunohistochemical analysis. Tumor-to-blood concentration ratios of ^{11}C-Gly-Sar increased in a time-dependent manner and were much higher than unity. Most of the radioactivity found in the tumor tissue was recovered as the intact tracer. These results indicated that ^{11}C-Gly-Sar was taken up by the PEPTs in tumor xenografts. It is noteworthy that ^{11}C-Gly-Sar was minimally present in inflammatory tissues that expressed no PEPT1 or PEPT2 protein, whereas ^{18}F-FDG was highly accumulated, with the values of the selectivity index being $>$25.1 and 0.72 for ^{11}C-Gly-Sar and ^{18}F-FDG, respectively. The mRNAs of PEPT1 and PEPT2 were expressed in 27.6% and 93.1%, respectively, of the cancer cell lines examined in the present study. **Conclusion:** The present study indicates that ^{11}C-Gly-Sar is a promising tumor-imaging agent and is superior to ^{18}F-FDG for distinguishing between tumors and inflammatory tissue. Because PEPTs were ubiquitously expressed in various types of tumor cells examined, ^{11}C-Gly-Sar could be useful for the detection of many types of cancers.

Key Words: H^+/peptide transporter; PEPT1; PEPT2; peptide transport activity; dipeptide PET tracer; ^{11}C-glycylsarcosine; cancer detection

J Nucl Med 2008; 49:615–622
DOI: 10.2967/jnumed.107.048231

The H^+/peptide transporters (PEPTs) PEPT1 (*SLC15A1*) and PEPT2 (*SLC15A2*) are members of the proton-coupled peptide transporter SLC15A family. In healthy humans, expression of PEPT1 is restricted to the small intestinal epithelial cells, the brush-border membrane of epithelial cells in the kidney proximal tubule S1 segment, and the apical membrane of bile duct epithelial cells (*1*). PEPT1 has enormous potential as an oral drug delivery target, because it also mediates the intestinal absorption of peptide-mimetic and nonpeptide substrates, in addition to numerous peptides derived from dietary proteins (*2,3*). A higher-affinity isoform, PEPT2, is localized in the brush-border membrane of S2 and S3 segment cells of the proximal tubule, lung, mammary gland, and choroid plexus, as well as in glial cells in the central nervous system (*4*). PEPT2 also transports various peptides and peptide-mimetics (*5*). One of the peptide-mimetics, 5-aminolevulinic acid, which has been used as a photosensitizer and also to guide the surgical resection of glioblastoma multiforme (*6*), is a substrate of PEPT1 (*7*) and PEPT2 (*8*). Antitumor agent ubenimex ((−)-*N*-[-(2*S*,3*R*)-3-amino-2-hydroxy-4-phenylbutyryl]-L-leucine), which induces apostosis in glioma (*9*), is also a substrate of PEPTs (*10*). In our previous study, repeated oral Ubenimex administration dramatically suppressed the growth of HeLa cells expressing human PEPT1 inoculated into mice (*11*). These observations suggest that PEPTs could be responsible for peptide transport activity in cancer cells.

Received Oct. 16, 2007; revision accepted Dec. 10, 2007.
For correspondence or reprints contact: Akira Tsuji, PhD, Laboratory of Innovative Pharmaceutics, Graduate School of Natural Science and Technology, Kanazawa University, Kakuma-machi, Kanazawa, Ishikawa 920-1192, Japan
E-mail: tsuji@kenroku.kanazawa-u.ac.jp

We have previously reported that a peptide transport activity exists in the human fibrosarcoma cell line HT1080 but does not exist in the normal fibroblast cell line IMR-90 cells (*12*). Gonzalez et al. reported that human pancreatic carcinoma cell lines AsPC-1 and Capan-2 also possess peptide transport activity and express PEPT1 (*13*). Subsequently, our group (*11*) and Knütter et al. (*14*) reported that human gastric cancer cell line MKN45, human osteosarcoma cell line MG-63, human bladder cancer cell line T24, and human extrahepatic cholangiocarcinoma cell line SK-ChA-1 also exhibit peptide transport activity. These findings suggest that the PEPTs may be a promising target for cancer imaging using PET.

It is noteworthy that many PET tracers used for cancer detection are thought to be substrates of specific transporters. For example, ^{18}F-FDG is a substrate of GLUT1 (*SLC2A1*) (*15,16*). 3′-Deoxy-3′-^{18}F-fluorothymidine (^{18}F-FLT), a thymidine analog, is a substrate of ENT1 (*SLC29A1*) (*17*). Tyrosine derivatives, such as *O*-(2-^{18}F-fluoroethyl)-L-tyrosine and *O*-^{11}C-methyl-L-tyrosine (*18,19*), may be substrates of LAT1 (*SLC7A5*) coupled with 4F2hc (*SLC3A2*) (*20*). These examples suggest that strategies using novel PET tracers targeting transporters expressed in tumors have potential value for cancer detection.

We hypothesized that PEPTs would be a suitable target for cancer detection using a peptide-based PET probe. Such a peptide-based PET probe may also be useful to distinguish tumors from inflammatory tissues, because, to our knowledge, there is no report of peptide transport activity in inflammatory tissues. Therefore, we examined the feasibility of using the peptide transport activity in cancer cells for imaging the tumors in tumor-bearing mice. Because the tissue localizations of PEPTs in mice are similar to those in humans (*21–24*), mice were expected to be a suitable model to evaluate peptide tracer characteristics. Recently, ^{11}C-glycylsarcosine (^{11}C-Gly-Sar) was reported as a PET tracer that can evaluate PEPT function (*25*). We describe here the use of ^{11}C-Gly-Sar as a PET tracer targeted to the PEPTs for cancer detection in mice.

MATERIALS AND METHODS

Animals and Cells

Male athymic mice (CAnN.Cg-*Foxn1^{nu}*/CrlCrlj) were obtained from Charles River Laboratories Japan, Inc. CRL-1682 AsPC-1 cells (American Type Culture Collection [ATCC]) were cultured in RPMI+GlutaMAX medium (Invitrogen Japan K.K.) containing 10% fetal bovine serum (Hyclone), 2 mM glutamine, 10 mM *N*-(2-hydroxyethyl)piperazine-*N*′-(2-ethanesulfonic acid) (HEPES), 1 mM sodium pyruvate, and 1.5 g/L bicarbonate. CRL-1435 PC-3 cells (ATCC) were cultured in F12 Kaighn's medium (Invitrogen) containing 10% fetal bovine serum. JCRB0254 MKN45 cells (Japanese Collection of Research Bioresources [JCRB] Cell Bank) were cultured in RPMI+GlutaMAX (Invitrogen) containing 10% fetal bovine serum. Other cell lines were obtained from the Cell Engineering Division of RIKEN BioResource Center.

Transplantation

The cells for xenotransplantation were grown to 95% confluence and then trypsinized (TrypLE Express; Invitrogen), and the single-cell suspension was centrifuged at 90*g* at 4°C for 5 min. The cell pellet was suspended directly with ice-cold PBS(−) (Invitrogen), which was followed by addition of the same volume of ice-cold liquid Matrigel (Becton-Dickinson). Adult mice (5 wk old) were injected subcutaneously with 5×10^6 AsPC-1 cells or 1×10^6 PC-3 and MKN45 cells and maintained for 2 wk after xenotransplantation; the mice were then used for experiments at 7 wk of age (body weight, 22.6 ± 1.5 g). Mice were maintained and handled in accordance with the recommendations of the National Institutes of Health, and animal experiments were performed in compliance with the requirements of the Animal Ethics Committee of The Medical and Pharmacologic Research Center Foundation.

Chemicals

^{3}H-Glycylsarcosine (18.5 GBq/mmol, Moravek Biochemicals Inc.) was obtained from Daiichi Pure Chemicals Co., Ltd. Oil of turpentine was purchased from Wako Pure Chemical Industry. Novo-Heparin was purchased from Mochida Pharmaceutical Co., Ltd. All other reagents were of the highest grade available.

Synthesis of Labeled Compound

The synthesis of ^{11}C-Gly-Sar reported by Nabulusi et al. (*25*) was modified slightly. The synthetic route for ^{11}C-Gly-Sar is indicated in Figure 1. The crude intermediate ^{11}C-1-methyl-2,5-piperazinedione was synthesized from glycylglycine ethyl ester hydrochloride using ^{11}C-methyl triflate according to the reported method (*25*). The reaction mixture was purified with a high-performance liquid chromatography (HPLC) system and eluted with 25 mM NH_4OAc (flow rate, 4.0 mL/min; column: DAISOPAK, SP-120-5-ODS-BP 10 × 250 mm; Daiso Chemical Co., Ltd.) to give a fraction containing ^{11}C-1-methyl-2,5-piperazinedione, which was collected in a reaction vessel containing 5N NaOH (120 μL). The mixture was heated to 140°C for 10 min and then cooled to ambient temperature. To this solution, 0.2 M Na_2HPO_4 (3 mL) was added and the mixture was passed through a sterile 0.22-μm filter (Millex GV; Millipore Corp.) to give ^{11}C-Gly-Sar as an injectable solution. The total synthesis time was 41 min from the end of bombardment. The decay-corrected radiochemical yield was 9.3%, the radiochemical purity was >97%, and the specific activity was 52.5 GBq/μmol.

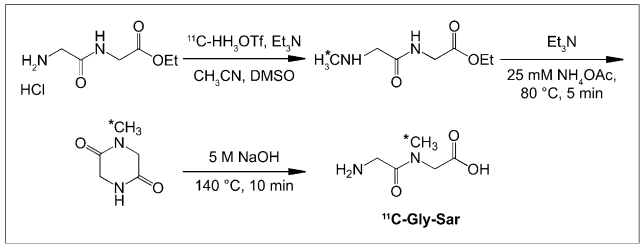

FIGURE 1. Synthetic route for ^{11}C-Gly-Sar. Synthesis of ^{11}C-Gly-Sar as reported by Nabulusi et al. (*25*) was modified slightly. Asterisk denotes position of ^{11}C labeling. DMSO = dimethyl sulfoxide.

Tissue Distribution Assay

The radiolabeled compound (0.7–29.8 MBq) dissolved in 150 μL of physiologic saline (Otsuka Pharmaceutical Factory, Inc.) was injected into each mouse through the tail vein. The animals were killed by decapitation at 5, 15, 30, and 60 min after injection; samples of blood, brain, heart, lung, liver, pancreas, kidney, bone, muscle, and tumor were rapidly removed and weighed, and the radioactivity was measured with a γ-counter (Wizard3, Wallac). Tracer uptake by various organs was quantified as dimensionless standardized uptake values (SUVs) using the formula: SUV = (Bq per gram of tissue/Bq injected per gram of body weight). For metabolite analysis of Gly-Sar, athymic mice bearing AsPC-1 cells were injected intravenously with 150 μL of ^{3}H-Gly-Sar (185 kBq/mouse) through the tail vein. The mice were immediately decapitated 60 min after receiving the intravenous dose of ^{3}H-Gly-Sar, and tissue samples were collected. The heparinized blood (Novo-Heparin, 5 U/mL of blood) was centrifuged to separate the plasma and weighed, and the tumor tissues were homogenized in an Ultra-Turrax T8 homogenizer (IKA-Werke GmbH & Co. KG) on ice. Acetonitrile was then added to plasma or tumor samples (sample/acetonitrile, 1:1, w/w), which was followed by centrifugation. Aliquots of 100 μL of supernatant were analyzed by reverse-phase HPLC, using a Shimadzu LC-6A pump, CTO-2A column oven, and SCL-6A system controller (Shimadzu Corp.). ^{3}H-Gly-Sar was separated on a YMC-Pack CN S-5 column (5 μm, 4.6 × 150 mm; YMC Co., Ltd.). Isocratic elution was performed by mixing acetonitrile and water containing 5 mM sodium dodecyl sulfate and 50 mM sodium dihydrogen phosphate adjusted to pH 2.6 with phosphate (5:95), at a constant flow rate of 1.0 mL/min. The retention time of ^{3}H-Gly-Sar was 4.6 min. Radioactivity of the collected ^{3}H-Gly-Sar fraction was measured with an LSC-5200 liquid scintillation counter (Aloka Co., Ltd.).

Whole-Body Imaging of Tumor-Bearing Mice

Kinetics and biodistribution patterns of each radiolabeled compound were determined with a positron planar imaging system (PPIS) (IPS-1000-6XII, Hamamatsu Photonics K.K.) (*19*). Mice anesthetized with sevoflurane (Maruishi Pharmaceutical Co., Ltd.) were positioned with the spine on an acrylic plate and placed on the midplane between the 2 opposing detectors arranged in a horizontal mode. ^{11}C-Gly-Sar at a dose of 5 MBq was intravenously injected into each mouse from the tail vein. The data were acquired with a 1-min time-frame interval for 60 min, and 6 summation images were created every 10 min.

Inflammation Model

For evaluation of tracer accumulation in inflammatory tissue, mice were subcutaneously administered 50 μL of oil of turpentine, and the tracer uptake was measured 3 d after injection (*19*). The selectivity index was defined as (tumor uptake − muscle uptake)/(inflammation uptake − muscle uptake)—that is, tumor-to-inflammation ratio corrected for background radioactivity.

Immunohistochemical Study of Expression of PEPT1 and PEPT2 in Tumor Xenografts and in Inflammatory Tissue

To examine PEPT1 and PEPT2 protein expression in xenografts of tumor-bearing mice, postmortem tumor, inflammatory, and normal tissues were harvested, embedded in OTC compound (Tissue-Tek; Sakura Finechemical Co., Ltd.), and fixed with paraformaldehyde. They were then frozen and cut into 10-μm sections with a Tissue-Tek cryostat. After incubation with a PEPT1- or PEPT2-specific polyclonal antibody (Santa Cruz Biotechnology, Inc.) at a dilution of 1:100 or 1:400, respectively, PEPT1 or PEPT2 immunoreactivity was visualized by reaction with EnVision (DaKoCytomation) or biotinylated antigoat IgG (Vector Laboratories), respectively. The specimens were examined with a Biozero microscope (Keyence Corp.). The objective lens was a Plan Apo 20 × /0.75 (Nikon Corp.).

Cellular Uptake Study

For the cellular uptake study, cancer cells were seeded at a density of 5.0×10^{4} (AsPC-1) or 2.0×10^{4} (PC-1 and MKN45) cells per well on 96-well plates (Nalge Nunc International K.K.) and grown for 2 d. The passage numbers were in the ranges of 4–7 for AsPC-1, 9–12 for PC-3, and 8–11 for MKN45 cells. Uptake of 2 μM ^{3}H-Gly-Sar by the cultured cells was examined at 37°C, pH 6.0 or 7.4. The procedures of the uptake experiments were as described previously (*12*). The radioactivity was determined using an LSC-6100 liquid scintillation counter (Aloka Co., Ltd.). Uptake of ^{3}H-Gly-Sar was described as uptake clearance (μL/min/mg protein), defined as the value obtained by dividing the uptake rate (nmol/min/mg protein) by the ^{3}H-Gly-Sar concentration in the uptake medium (2 μM).

Quantitative Real-Time Poymerase Chain Reaction (RT-qPCR) Analysis

Quantification of the messenger RNAs (mRNAs) coding for human PEPT1 and PEPT2 in cancer cell lines was performed by using the LightCycler system (Roche Diagnostics) with the LightCycler FastStart DNA MasterPLUS HybProbe (Roche Diagnostics) according to the manufacturer's protocol. The PEPT1 and PEPT2 primers were designed and synthesized by TaKaRa Bio Inc. Hybridization probe sets (Fluorescein Probe and LCRed640 Probe) were designed and synthesized by Nihon Gene Research Laboratories Inc. The absolute concentration of the external standard was measured with a NanoDrop ND-1000 (NanoDrop Technologies).

Statistical Analysis

Results are presented as mean ± SD. Differences of SUVs in the various tissues and in tissue-to-blood ratios were compared using ANOVA, which was followed by the Dunnett or Scheffé post hoc tests (KaleidaGraph; Synergy Software). Comparisons between conditions were performed using an unpaired, 2-tailed Student t test. A P value < 0.05 was considered significant.

RESULTS

Whole-Body PPIS Imaging of ^{11}C-Gly-Sar in Tumor-Bearing Mice

To evaluate ^{11}C-Gly-Sar as a tumor-detecting agent, whole-body PPIS imaging (static collection, 10 min) with ^{11}C-Gly-Sar in athymic mice bearing pancreatic cancer AsPC-1 was performed. Data are displayed as the images accumulated every 10 min, up to 60 min after injection (Fig. 2A). ^{11}C-Gly-Sar showed clear delineation of the tumor in the right hind limb compared with the contralateral normal tissue (left hind limb). Remarkable accumulation of ^{11}C-Gly-Sar in the tumor was apparent from an early time point after injection. Prostate cancer PC-3 (Fig. 2B) and gastric cancer MKN45 (Fig. 2C) were also well visualized by ^{11}C-Gly-Sar injection. The kidneys were

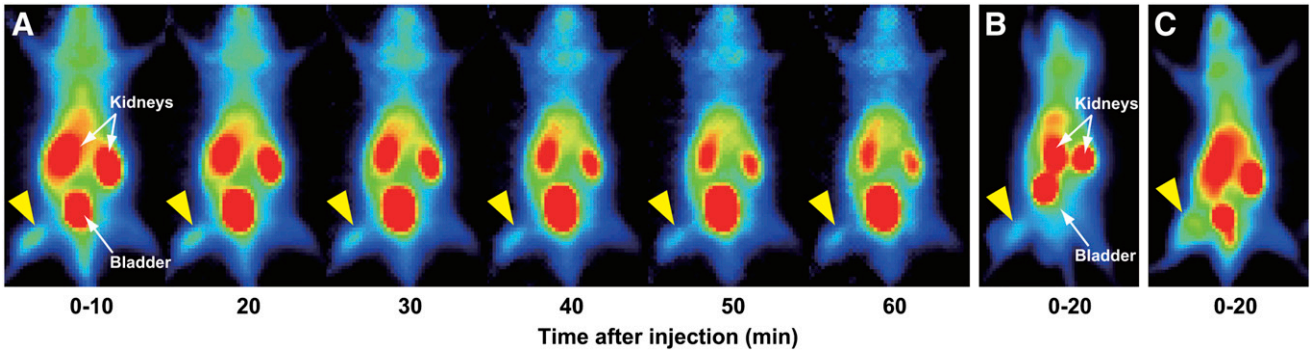

FIGURE 2. Whole-body PPIS imaging of ^{11}C-Gly-Sar in tumor-bearing mice. Mice, inoculated subcutaneously with AsPC-1 (A), PC-3 (B), or MKN45 (C) cells on right side of hind limb and anesthetized with Sevoflurane, were positioned spine down on an acrylic plate and placed on midplane between 2 opposing detectors arranged in a horizontal mode. ^{11}C-Gly-Sar (5 MBq) was injected intravenously into each mouse via tail vein. Data were acquired with a 1-min time-frame interval for 60 min after injection, and 6 summation images were created every 10 min (A). Merged images at 0–20 min are shown (B and C). Yellow arrowhead indicates tumor.

found to be the primary sites of uptake of ^{11}C-Gly-Sar (Fig. 2), as reported previously (*25*) after intravenous administration. ^{14}C-Gly-Sar was reported to be mainly excreted in urine (*8*), and ^{11}C-Gly-Sar was rapidly accumulated in the bladder (Fig. 2). HPLC with radiochemical detection demonstrated that 72.9% ± 8.7% (mean ± SD, $n = 5$) of the radioactivity recovered in the AsPC-1 xenograft at 60 min after an intravenous bolus dose of ^{3}H-Gly-Sar was that of intact Gly-Sar.

Biodistribution of ^{11}C-Gly-Sar in Tumor-Bearing Mice

Figure 3 shows the biodistribution of ^{11}C-Gly-Sar in athymic mice bearing AsPC-1 (Fig. 3A), PC-3 (Fig. 3B), and MKN45 (Fig. 3C). Significant accumulation of ^{11}C-Gly-Sar in the tumor was detected from an early time point after injection, and tumor uptakes of ^{11}C-Gly-Sar were comparable during 5–60 min after injection (Fig. 3). The SUVs of ^{11}C-Gly-Sar in AsPC-1, PC-3, and MKN45 xenografts at 60 min after intravenous dosing were 0.70 ± 0.11, 0.53 ± 0.05, and 0.42 ± 0.03 (mean ± SD, $n = 5$), respectively. The SUVs of ^{11}C-Gly-Sar in muscle ranged from 0.11 to 0.22 at 60 min. The tracer uptake values obtained from various tissues at 60 min after injection in AsPC-1 xenograft-bearing mice were initially tested using overall repeated-measures ANOVA, which was found to be significant ($F_{9,39} = 76.1$, $P < 0.0001$). The post hoc test revealed that tracer uptake in the tumor tissue was significantly higher than that in blood ($P = 0.0011$), brain ($P = 0.0005$), muscle ($P = 0.0020$), and heart ($P = 0.012$) but was lower than that in pancreas ($P < 0.0001$) or kidney ($P < 0.0001$). No significant differences in the tracer uptake were found between tumor tissue and bone ($P = 0.19$), lung ($P = 1.0$), or liver ($P = 1.0$) (Fig. 3A). Similar results were obtained in PC-3- or MKN45-bearing mice (Figs. 2B and 2C). The T/B and T/M ratios, diagnostically important parameters, were elevated until 30 min after intravenous injection, in contrast to the M/B ratio (Figs. 2A–2C, insets). The T/B ratio of ^{11}C-Gly-Sar was significantly higher than the M/B ratio ($P < 0.0001$) from 5 to 60 min after intravenous injection.

Immunohistochemistry of PEPT1 or PEPT2 in Human Cancer Xenografts Implanted in Mice and Inflammatory Tissue

The expression of PEPT1 or PEPT2 in cancer xenografts inoculated into athymic mice was examined by immunohistochemistry using specific antibodies. Strong positive signals with antihuman PEPT1 or antihuman PEPT2 antibody were observed in AsPC-1, PC-3, and MKN45 xenografts (Fig. 4), shown as brown arrowheads. In inflammatory tissues that were induced subcutaneously with oil of turpentine, specific signals for PEPT1 and PEPT2 were negligible (Fig. 4B). Positive signals for PEPT1 and PEPT2 were observed in the kidney (positive controls), whereas no signals were observed in the muscle (negative controls) (Fig. 4C).

In Vitro Uptake of ^{3}H-Gly-Sar by Cancer Cell Lines

The uptake of 2 μM ^{3}H-Gly-Sar in 10 min by cancer cells was measured in the absence or presence of unlabeled Gly-Sar (20 mM). The initial uptake clearances were 3.88 ± 0.25 or 0.94 ± 0.20 (AsPC-1), 1.39 ± 0.13 or 1.22 ± 0.11 (PC-3), and 1.64 ± 0.03 or 0.77 ± 0.08 (MKN45) μL/min/mg protein (mean ± SD, $n = 4$), respectively. ^{3}H-Gly-Sar uptake observed in AsPC-1 cells was pH-dependent, with saturable uptake values (μL/min/mg protein) of 2.94 ± 0.32 and 1.62 ± 0.13 at pH 6.0 and 7.4, respectively.

Accumulation of ^{18}F-FDG and Lack of Accumulation of ^{11}C-Gly-Sar in Inflammatory Tissues

No specific uptake of ^{11}C-Gly-Sar was found in inflammatory tissues, whereas ^{18}F-FDG had a higher accumulation in inflammatory tissue than that in tumor tissue in mice inoculated with AsPC-1 cells (Fig. 5). The mice without injection of turpentine oil are shown as controls. The tissue distribution of ^{11}C-Gly-Sar in inflammatory tissue was compared with that of ^{18}F-FDG in athymic mice bearing

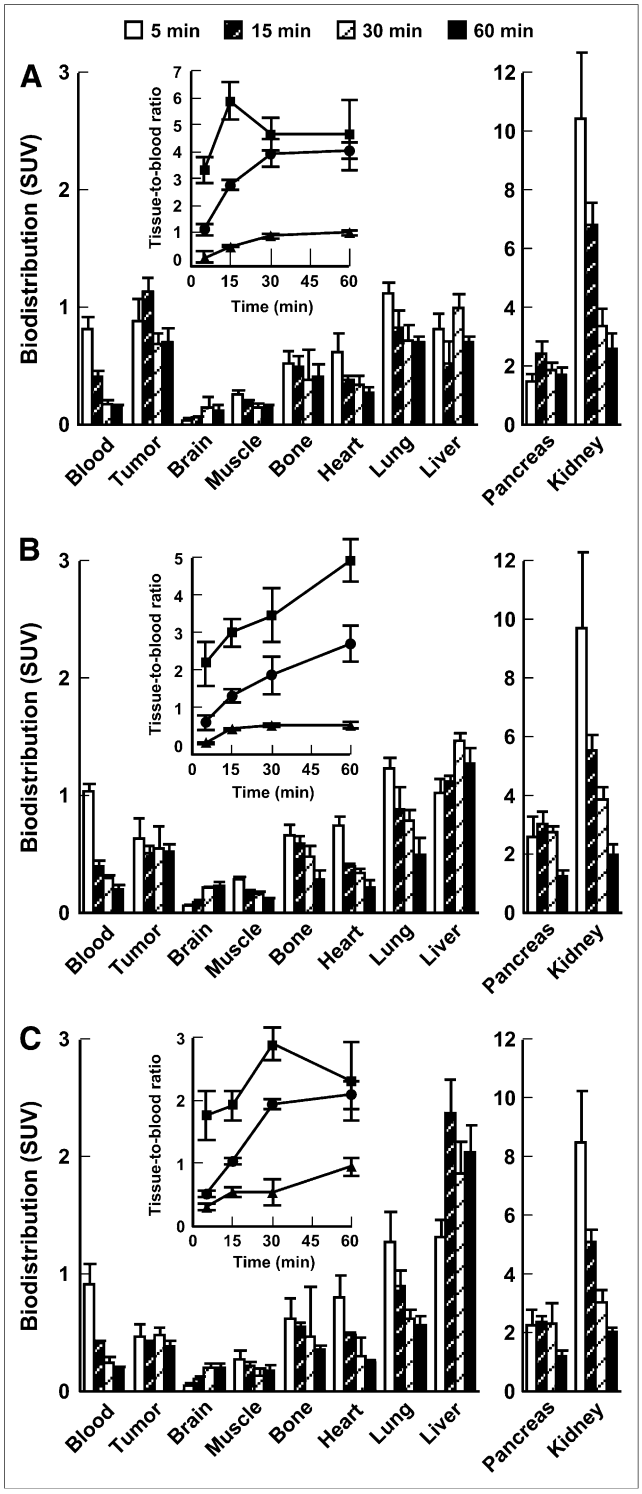

FIGURE 3. Biodistribution of ^{11}C-Gly-Sar as determined by radioactivity assay in tumor-bearing mice. Postmortem tissues were harvested at 5 (white bars), 15 (black hatched bars), 30 (white hatched bars), and 60 (black bars) min after intravenous injection of ^{11}C-Gly-Sar in AsPC-1-bearing (A), PC-3-bearing (B), and MKN45-bearing (C) mice (n = 5). Uptakes are expressed as mean ± SD of SUV. (Insets) Tumor-to-blood (circles), tumor-to-muscle (squares), and muscle-to-blood (triangles) SUV ratios of ^{11}C-Gly-Sar are plotted against the time period after injection.

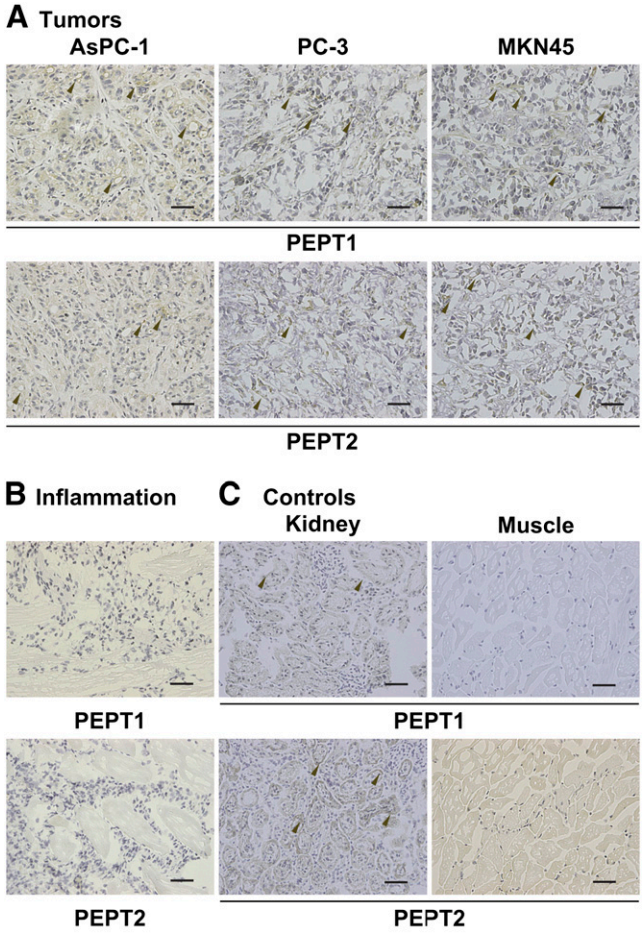

FIGURE 4. Immunohistochemistry of PEPT1 or PEPT2 in human cancer xenografts implanted in mice and in inflammatory tissue. Microscopic images were obtained of sections of human pancreatic cancer AsPC-1, prostate cancer PC-3, and gastric cancer MKN45 xenografts (A) and inflammatory tissue (B) at 3 d after injection of turpentine oil. Immunoreactivity of antihuman PEPT1 or antihuman PEPT2 antibodies was also examined in tissue sections of positive control (kidney) or negative control (muscle) (C). Tissue sections were counterstained with 4′-6′-diamidino-2-phenylindole (DAPI) (blue) to show cell nuclei (bars = 50 μm).

AsPC-1 (Fig. 5B). One-way factorial ANOVA ($F_{2,15}$ = 54.2, $P < 0.0001$) and the Scheffé post hoc test revealed that the inflammation-to-blood ratio (I/B) and M/B of ^{11}C-Gly-Sar were not significantly different ($P = 0.98$). The I/B ratio of ^{11}C-Gly-Sar was significantly smaller than the T/B ratio ($P < 0.0001$). However, ^{18}F-FDG accumulation was 6.8-fold higher in inflammatory tissue than in the non-inflamed contralateral muscle ($P < 0.0001$). The selectivity index (tumor-to-inflammatory tissue ratio corrected for uptake in healthy muscle) was >25.1 for ^{11}C-Gly-Sar and 0.72 ± 0.13 for ^{18}F-FDG, respectively. The SD for ^{11}C-Gly-Sar could not be calculated because, in some animals, tracer uptake in inflammatory tissue was smaller than that in the contralateral healthy muscle. The difference in SUV between ^{11}C-Gly-Sar and ^{18}F-FDG in the tumor was not significant ($P = 0.95$). Furthermore, The T/B ratios of

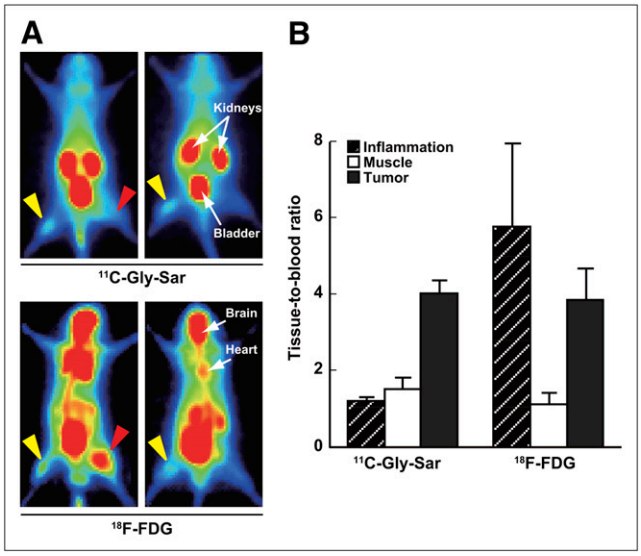

FIGURE 5. Accumulation of ^{18}F-FDG but absence of accumulation of ^{11}C-Gly-Sar in inflammatory tissues in mice. (A) Mice were inoculated subcutaneously with AsPC-1 cells (yellow arrowheads) in right side of hind legs with or without subcutaneous inoculation of oil of turpentine (50 μL) in left hind legs at 3 d before tracer injection (red arrowheads). Mice were imaged by PPIS with ^{11}C-Gly-Sar and ^{18}F-FDG injection, and accumulated images were created from 0 to 20 and 41 to 60 min, respectively, after injection. (B) I/B (hatched bars), M/B (white bars), and T/B (black bars) ratios of ^{11}C-Gly-Sar and ^{18}F-FDG at 60 min after injection are presented in E. Mean ± SD (n = 5).

^{11}C-Gly-Sar and ^{18}F-FDG were not significantly different (Fig. 5B, P = 0.71).

Expression of mRNA of PEPT1 and PEPT2 in Various Human Cancer Cell Lines

Quantitative RT-PCR was performed by using the LightCycler system with HybProbes specific for each mRNA transcript. mRNAs coding for human PEPT1 and PEPT2 in 58 human cancer cell lines were examined (Table 1). The expression levels of mRNA of PEPT1 were high in renal cell carcinoma VMRC-RCW, pancreatic adenocarcinoma AsPC-1 cells, ovary serous adenocarcinoma JHOS-2, ovary clear cell carcinoma JHOS-8, and poorly differentiating gastric adenocarcinoma MKN45 cells. The percentage of cell lines containing PEPT1 mRNA over the quantification limit was 27.6%. On the other hand, mRNA levels of PEPT2 were above the quantification limit in 54 of 58 cell lines (93.1%). Notably, poorly differentiated esophageal squamous cell carcinoma TE-9, tongue squamous cell carcinoma HSC-3, primitive neuroectodermal tumor cell line derived from kidney (FU-RPNT-2), epidermoid carcinoma A431, and ovary serous adenocarcinoma JHOS-2 exhibited high levels of PEPT2 mRNA.

DISCUSSION

This study demonstrates that PEPTs are promising targets for cancer detection. We were able to detect human pancreatic cancer, prostate cancer, and gastric cancer in mice by using a prototypical positron probe for the PEPT ^{11}C-Gly-Sar. ^{11}C-Gly-Sar was also able to distinguish between tumor and inflammatory tissue, in combination with ^{18}F-FDG.

Whole-body PPIS imaging effectively visualized an AsPC-1 tumor xenograft when ^{11}C-Gly-Sar was injected into mice as a PET tracer (Fig. 2). The tissue distribution study of ^{11}C-Gly-Sar revealed that background accumulation of the tracer was quite low, presumably because of restricted functional expression of PEPTs in tissues (Fig. 2). The SUV of ^{11}C-Gly-Sar in the tumor was significantly larger than that in blood, brain, muscle, bone, or heart at 15 min after injection (Fig. 3). Clear tumor visualization from the early period after injection is a prominent characteristic of this tracer. Considering that most of the radioactivity that appeared in the tumor xenograft was due to intact Gly-Sar, it can be assumed that the rapid accumulation of the tracer in tumors occurs not because of metabolic trapping but as a result of PEPT-mediated uptake. Imaging of tumor lesions with good contrast at an early time after tracer injection would be an advantage in clinical application.

Subsequently, to corroborate the potential usefulness of ^{11}C-Gly-Sar in cancer detection, we performed whole-body PPIS imaging and biodistribution studies in mice with other xenografts, using gastric cancer MKN45 cells possessing peptide transport activity in vitro (*11,26*) and prostate cancer PC-3 (Fig. 2), where the use of ^{18}F-FDG is unfavorable because of its relatively low uptake in these cancers (*27*). As shown in Figure 2, specific visualization of MKN45 and PC-3 xenografts was observed after injection of ^{11}C-Gly-Sar. The SUVs in xenografts of MKN45 or PC-3 tumor were similar to that in AsPC-1 tumor (Fig. 3). Our imaging and biodistribution studies revealed that ^{11}C-Gly-Sar was specifically taken up by the tumors in vivo. The detection of PEPT1 and PEPT2 proteins in tumor tissue sections, but not in muscle (Fig. 4), together with the fact that SUVs were consistently higher in the tumor tissues but much lower in the muscle (Fig. 3), indicates that the uptake of ^{11}C-Gly-Sar in these tumors was mediated by these PEPTs.

The in vitro transport activities observed in AsPC-1 cells and MKN45 cells, and the mRNA and protein expression levels of PEPTs (Table 1 and Fig. 4) were also consistent with the in vivo imaging data (Fig. 2). Thus, the accumulations of ^{11}C-Gly-Sar in these 2 xenografts were concluded to be due to uptake by PEPTs, supporting our hypothesis that targeting of peptide transporter(s) with ^{11}C-Gly-Sar is a useful strategy for visualizing tumors in vivo by means of PET. On the other hand, there was an apparent discrepancy in the case of PC-3 between in vivo imaging results (Fig. 2) and in vitro cellular uptake data: Although mRNAs of both PEPT1 and PEPT2 (Table 1), and in vitro cellular uptake of ^{3}H-Gly-Sar by PC-3 cells, were negligible, the tumor xenograft was clearly visualized by ^{11}C-Gly-Sar in PC-3 xenografts (Fig. 2). On the basis of the fact that PEPT1 and PEPT2 proteins were clearly detected in the in vivo PC-3

TABLE 1
mRNA Expression of PEPT1 and PEPT2 in Various Human Cancer Cell Lines

Source tissue & cell name	PEPT1	PEPT2	Source tissue & cell name	PEPT1	PEPT2	Source tissue & cell name	PEPT1	PEPT2
Lung			Bladder			Brain		
A549	UQL	39 ± 10	T24	0.2 ± 0.0	2 ± 0	T98G	UQL	UQL
PC-10	UQL	53 ± 2	Uterus			CCF-STTG1	UQL	11 ± 5
Lu99B	UQL	23 ± 5	JHUEM-7	UQL	12 ± 4	IMR-32	UQL	82 ± 31
T3 M-12	UQL	29 ± 27	JHUCS-3	1.5 ± 0.0	41 ± 15	SCCH-26	UQL	166 ± 0
EBC-1	UQL	76 ± 15	Cervix			Pleural effusion		
LK-2	1.1 ± 0.2	19 ± 10	HeLa	UQL	29 ± 6	U-937	UQL	333 ± 99
Kidney			Ovary			Malignant pleural mesothelioma		
ACHN	UQL	29 ± 2	JHOS-2	63.2 ± 8.7	1,887 ± 429	ACC-MESO-1	UQL	151 ± 53
VMRC-RCW	279.4 ± 72.7	35 ± 11	JHOS-4	0.5 ± 0.1	361 ± 86	Peripheral blood		
FU-RPNT-2	UQL	3,118 ± 16	JHOS-8	29.1 ± 3.3	UQL	PCM6	0.8 ± 0.4	188 ± 6
Pancreas			JHOM-2B	1.3 ± 0.2	52 ± 21	Blood		
PK-45-H	UQL	UQL	KGN	UQL	97 ± 46	EoL-1	UQL	577 ± 129
PK-1	UQL	1,550 ± 9	Connective tissue			KU812F	UQL	248 ± 55
AsPC-1	105.3 ± 51.3	93 ± 4	HT1080	UQL	8 ± 1	OIH-1	UQL	406 ± 7
Stomach			Epidermis			HL-60	UQL	125 ± 36
MKN45	40.7 ± 4.4	3 ± 2	A431	UQL	3,037 ± 131	THP-1	UQL	278 ± 124
LMSU	UQL	UQL	Esophagus			Jurkat	UQL	118 ± 33
AZ521	UQL	4 ± 0	TE-15	UQL	49 ± 7	MOLT-4	UQL	59 ± 12
KATO III	0.1 ± 0.0	10 ± 1	TE-5	UQL	162 ± 79	Bone marrow		
Liver			TE-9	UQL	3,640 ± 364	HYT-1	UQL	1,392 ± 708
HepG2	UQL	24 ± 3	Thyroid			Bone		
HuH-6	UQL	15 ± 4	HTC/C3	1.4 ± 0.3	76 ± 22	MG-63	UQL	22 ± 7
Bile duct			Oral, thoracic cavity meta			Skin		
HuCCT1	7.7 ± 1.6	43 ± 12	CJM	UQL	608 ± 224	SK-Mel-28	UQL	2 ± 0
Mammary gland			Gingiva					
T47-D	UQL	1 ± 0	Ca9-22	UQL	842 ± 376			
CRL1500	UQL	432 ± 2	Tongue					
Prostate			HSC-3	0.5 ± 0.6	3,556 ± 1,534			
PC-3	0.1 ± 0.0	11 ± 2						

UQL = under quantification limit (>0.05 copy/ng total RNA for PEPT1; >0.5 copy/ng total RNA for PEPT2).

Expression levels are reported as copy/ng total RNA (mean ± SD; $n = 4$). Determinations were performed in duplicate on each sample by 2-step real-time quantitative PCR using complementary DNA obtained by reverse transcription from total RNA of human cancer cell lines.

xenograft (Fig. 4), we speculate that PEPTs might have been induced by the inoculation of the cells into the mice in vivo, leading to uptake of ^{11}C-Gly-Sar and consequently resulting in the detection of the cancer by in vivo imaging. Further experiments are needed to examine the possible induction of these PEPTs in the PC-3 xenograft and its physiologic role in vivo. PEPT1 is a high-capacity, low-affinity transporter, in contrast to PEPT2, which is a low-capacity, high-affinity transporter (*4*). The contribution ratio of PEPT1 and PEPT2 to the uptake of ^{11}C-Gly-Sar by tumors in vivo was not determined in this study and should also be evaluated.

The vicinity of tumor tissues in vivo is known to be more acidic than that of normal tissue (*28*), and this acidic environment may favor the function of PEPTs, as transport of peptides is activated by an inwardly directed proton gradient (*29*). This idea was confirmed in the present study, because transport into AsPC-1 cells was almost 2 times larger at pH 6.0 than at pH 7.4. The relatively small accumulation of ^{11}C-Gly-Sar in inflammatory tissue (Fig. 5) suggests that ^{11}C-Gly-Sar may be an effective probe to distinguish tumors from the inflammatory tissues in vivo in combination with ^{18}F-FDG, at least for some cancers. Such tumor-specific imaging by ^{11}C-Gly-Sar is consistent with the absence of PEPTs in inflammatory tissue (Fig. 4) and is in marked contrast to the case of ^{18}F-FDG, which exhibited greater accumulation in inflammatory tissues than tumor xenograft (Fig. 5).

Another advantage of ^{11}C-Gly-Sar was the much smaller accumulation in the brain (Figs. 2 and 3). Accumulation of ^{11}C-Gly-Sar in the brain, which does not express PEPTs, was only 5% of ^{18}F-FDG uptake at 60 min ($P < 0.00001$). This result may imply that brain tumors could also be identified with peptide PET tracer. The marked accumulation of ^{11}C-Gly-Sar in the PC-3 xenograft (Fig. 2) suggested that this tracer may be suitable for detection of prostate cancer. Because ^{11}C- and ^{18}F-labeled choline has recently been used for prostate cancer imaging (*27,30–32*),

it would be interesting to compare the potential usefulness of the peptide tracer and choline analogs. It may be difficult to detect renal or bladder tumors with peptide tracers because of the high accumulation of these tracers in the clearance organs (Fig. 2) (*8,25*). Inoue et al. (*26*) reported that PEPT1 was induced by 5-fluorouracil treatment, in contrast to a decrease of GLUT1 at the mRNA and protein levels. ^{11}C-Gly-Sar may also be a promising tracer for assessment of the efficacy of chemotherapy with 5-fluorouracil, and this seems worthy of further study. Recently, Knütter et al. (*33*) developed a high-affinity transported substrate for PEPTs, Bip-Pro, which is a stable dipeptide. Bip-Pro will be also a valuable candidate for cancer detection by positron labeling as well as ^{11}C-Gly-Sar. As the tissue distributions of PEPTs in healthy mice are similar to those in healthy humans (*21–24*), ^{11}C-Gly-Sar-PET seems to be an excellent candidate for cancer detection in the clinical situation.

CONCLUSION

Our results indicate that the peptide PET tracer ^{11}C-Gly-Sar is a promising candidate for cancer detection. Unlike ^{18}F-FDG, this tracer can distinguish tumors from inflammatory tissues.

ACKNOWLEDGMENTS

The authors appreciate the excellent technical assistance of Mariko Hiraiwa in performing the quantitative RT-PCR and Masashi Yamamoto, Taishiro Kimura, Yasufumi Okano, Jun Mizusawa in the animal experiments. Complementary DNA synthesis was performed by Kaori Yoshino. We also thank Dr. Ichiro Matsunari for helpful discussions as well as a critique of the manuscript. This study was sponsored by Ishikawa prefectural government, Japan, and was also supported in part by a grant-in-aid for scientific research provided by the Ministry of Education, Culture, Sports, Science and Technology, Japanese Government.

REFERENCES

1. Herrera-Ruiz D, Knipp GT. Current perspectives on established and putative mammalian oligopeptide transporters. *J Pharm Sci.* 2003;92:691–714.
2. Daniel H. Molecular and integrative physiology of intestinal peptide transport. *Annu Rev Physiol.* 2004;66:361–384.
3. Sai Y, Tsuji A. Transporter-mediated drug delivery: recent progress and experimental approaches. *Drug Discov Today.* 2004;9:712–720.
4. Rubio-Aliaga I, Daniel H. Mammalian peptide transporters as targets for drug delivery. *Trends Pharmacol Sci.* 2002;23:434–440.
5. Biegel A, Gebauer S, Brandsch M, Neubert K, Thondorf I. Structural requirements for the substrates of the H^+/peptide cotransporter PEPT2 determined by three-dimensional quantitative structure-activity relationship analysis. *J Med Chem.* 2006;49:4286–4296.
6. Dolmans DE, Fukumura D, Jain RK. Photodynamic therapy for cancer. *Nat Rev Cancer.* 2003;3:380–387.
7. Doring F, Walter J, Will J, et al. Delta-aminolevulinic acid transport by intestinal and renal peptide transporters and its physiological and clinical implications. *J Clin Invest.* 1998;101:2761–2767.
8. Ocheltree SM, Shen H, Hu Y, Xiang J, Keep RF, Smith DE. Role of PEPT2 in the choroid plexus uptake of glycylsarcosine and 5-aminolevulinic acid: studies in wild-type and null mice. *Pharm Res.* 2004;21:1680–1685.
9. Schlapbach R, Fontana A. Differential activity of bcl-2 and ICE enzyme family protease inhibitors on Fas and puromycin-induced apoptosis of glioma cells. *Biochim Biophys Acta.* 1997;1359:174–180.
10. Tomita Y, Katsura T, Okano T, Inui K, Hori R. Transport mechanisms of bestatin in rabbit intestinal brush-border membranes: role of H^+/dipeptide cotransport system. *J Pharmacol Exp Ther.* 1990;252:859–862.
11. Nakanishi T, Tamai I, Takaki A, Tsuji A. Cancer cell-targeted drug delivery utilizing oligopeptide transport activity. *Int J Cancer.* 2000;88:274–280.
12. Nakanishi T, Tamai I, Sai Y, Sasaki T, Tsuji A. Carrier-mediated transport of oligopeptides in the human fibrosarcoma cell line HT1080. *Cancer Res.* 1997;57:4118–4122.
13. Gonzalez DE, Covitz KM, Sadee W, Mrsny RJ. An oligopeptide transporter is expressed at high levels in the pancreatic carcinoma cell lines AsPc-1 and Capan-2. *Cancer Res.* 1998;58:519–525.
14. Knütter I, Rubio-Aliaga I, Boll M, et al. H^+-Peptide cotransport in the human bile duct epithelium cell line SK-ChA-1. *Am J Physiol Gastrointest Liver Physiol.* 2002;283:G222–G229.
15. Avril N. GLUT1 expression in tissue and ^{18}F-FDG uptake. *J Nucl Med.* 2004;45:930–932.
16. Mochizuki T, Tsukamoto E, Kuge Y, et al. FDG uptake and glucose transporter subtype expressions in experimental tumor and inflammation models. *J Nucl Med.* 2001;42:1551–1555.
17. Perumal M, Pillai RG, Barthel H, et al. Redistribution of nucleoside transporters to the cell membrane provides a novel approach for imaging thymidylate synthase inhibition by positron emission tomography. *Cancer Res.* 2006;66:8558–8564.
18. Heiss P, Mayer S, Herz M, Wester HJ, Schwaiger M, Senekowitsch-Schmidtke R. Investigation of transport mechanism and uptake kinetics of O-(2-[^{18}F]fluoroethyl)-L-tyrosine in vitro and in vivo. *J Nucl Med.* 1999;40:1367–1373.
19. Tsukada H, Sato K, Fukumoto D, Nishiyama S, Harada N, Kakiuchi T. Evaluation of D-isomers of O-^{11}C-methyl tyrosine and O-^{18}F-fluoromethyl tyrosine as tumor-imaging agents in tumor-bearing mice: comparison with L- and D-^{11}C-methionine. *J Nucl Med.* 2006;47:679–688.
20. Kanai Y, Segawa H, Miyamoto K, Uchino H, Takeda E, Endou H. Expression cloning and characterization of a transporter for large neutral amino acids activated by the heavy chain of 4F2 antigen (CD98). *J Biol Chem.* 1998;273:23629–23632.
21. Hilgendorf C, Ahlin G, Seithel A, Artursson P, Ungell AL, Karlsson J. Expression of thirty-six drug transporter genes in human intestine, liver, kidney, and organotypic cell lines. *Drug Metab Dispos.* 2007;35:1333–1340.
22. Kim HR, Park SW, Cho HJ, et al. Comparative gene expression profiles of intestinal transporters in mice, rats and humans. *Pharmacol Res.* 2007;56:224–236.
23. Liang R, Fei YJ, Prasad PD, et al. Human intestinal H^+/peptide cotransporter: cloning, functional expression, and chromosomal localization. *J Biol Chem.* 1995;270:6456–6463.
24. Lu H, Klaassen C. Tissue distribution and thyroid hormone regulation of Pept1 and Pept2 mRNA in rodents. *Peptides.* 2006;27:850–857.
25. Nabulsi NB, Smith DE, Kilbourn MR. [^{11}C]Glycylsarcosine: synthesis and in vivo evaluation as a PET tracer of PepT2 transporter function in kidney of PepT2 null and wild-type mice. *Bioorg Med Chem.* 2005;13:2993–3001.
26. Inoue M, Terada T, Okuda M, Inui K. Regulation of human peptide transporter 1 (PEPT1) in gastric cancer cells by anticancer drugs. *Cancer Lett.* 2005;230:72–80.
27. Fricke E, Machtens S, Hofmann M, et al. Positron emission tomography with ^{11}C-acetate and ^{18}F-FDG in prostate cancer patients. *Eur J Nucl Med Mol Imaging.* 2003;30:607–611.
28. Izumi H, Torigoe T, Ishiguchi H, et al. Cellular pH regulators: potentially promising molecular targets for cancer chemotherapy. *Cancer Treat Rev.* 2003;29:541–549.
29. Fei YJ, Kanai Y, Nussberger S, et al. Expression cloning of a mammalian proton-coupled oligopeptide transporter. *Nature.* 1994;368:563–566.
30. Hara T, Bansal A, DeGrado TR. Choline transporter as a novel target for molecular imaging of cancer. *Mol Imaging.* 2006;5:498–509.
31. Kotzerke J, Prang J, Neumaier B, et al. Experience with carbon-11 choline positron emission tomography in prostate carcinoma. *Eur J Nucl Med.* 2000;27:1415–1419.
32. Price DT, Coleman RE, Liao RP, Robertson CN, Polascik TJ, DeGrado TR. Comparison of [^{18}F]fluorocholine and [^{18}F]fluorodeoxyglucose for positron emission tomography of androgen dependent and androgen independent prostate cancer. *J Urol.* 2002;168:273–280.
33. Knütter I, Hartrodt B, Toth G, et al. Synthesis and characterization of a new and radiolabeled high-affinity substrate for H^+/peptide cotransporters. *FEBS J.* 2007;274:5905–5914.